

Creep Properties Assessment of P92 Steel by Small Punch Creep Tests

G. S. Deshmukh¹ · M. L. Prasad¹ · D. R. Peshwe¹ · J. Ganesh Kumar² ·
M. D. Mathew² · G. Amarendra³

Received: 4 February 2015 / Accepted: 13 May 2015 / Published online: 17 July 2015
© The Indian Institute of Metals - IIM 2015

Abstract Small punch creep (SPC) tests have the potential as an alternative to conventional uniaxial creep tests when limited amount of material is available. This paper investigates the applicability of SPC to evaluate the creep deformation behavior of P92 steel. SPC results have been compared with uniaxial creep test results in order to establish the correlation between the two tests. Small punch tests on P92 steel have been performed at 600 °C in the load range of 1000–400 N. The load dependence of minimum deflection rate was found to obey Norton's power law but with a two slope behavior exhibiting distinct values of load exponents in the low and high load regimes. Transition in fracture mode of SPC specimens from ductile transgranular at high loads to brittle intergranular fracture at low loads was in accordance with the large variation in load exponent values. Monkman–Grant equation interrelating minimum deflection rate with rupture time has been found to be valid for SPC data. Correlations between SPC load and minimum deflection rate with uniaxial creep stress and minimum creep rate respectively, established based on empirical relations suggest the relevance of SPC for evaluating creep properties in relatively short time.

Keywords Small punch creep · P92 steel · Creep deformation

1 Introduction

The development of new generation high temperature materials for power plants has increased the demand for rapid screening of their mechanical properties. Coupled with this there is growing need for assessment of residual lifetime of in-service structural components in power plants and petro-chemical industries with a limited volume of material. In this context the development of miniaturized specimen tests have gained considerable importance over the past 30 years. A comprehensive summary of various miniaturized tests can be found in the review articles by Lucas [1, 2]. Amongst these, the small punch (SP) test formulated in early 1980s [3–7] has evolved as an innovative miniaturized technique to evaluate the mechanical performance of materials. The SP testing is a noninvasive technique as it requires very small amount of material for the test. Furthermore, SP test offers the potential to assess the properties of distinct microstructural regions like the heat affected zones in weld joints.

In SP test a small ceramic ball indenter penetrates through thin specimen of 0.5 mm thickness until it ruptures as shown in Fig. 1. There are two basic modes in which the SP test can be carried out: (i) constant deflection mode and (ii) constant load mode. The SP test conducted in constant deflection mode measures the force (F) as a function of indenter displacement and is similar to conventional tensile test. Manahan et al. [3] originally developed this test to analyze the mechanical performance of irradiated and unirradiated materials due to the constraints on the irradiation of standard size specimens. The applications of

✉ G. S. Deshmukh
gaurid2007@rediffmail.com

¹ Department of Metallurgical and Materials Engineering,
Visvesvaraya National Institute of Technology, Nagpur
440 010, India

² Mechanical Metallurgy Division, Indira Gandhi Centre for
Atomic Research, Kalpakkam 603 102, Tamilnadu, India

³ Materials Science Group, Indira Gandhi Centre for Atomic
Research, Kalpakkam 603 102, Tamilnadu, India

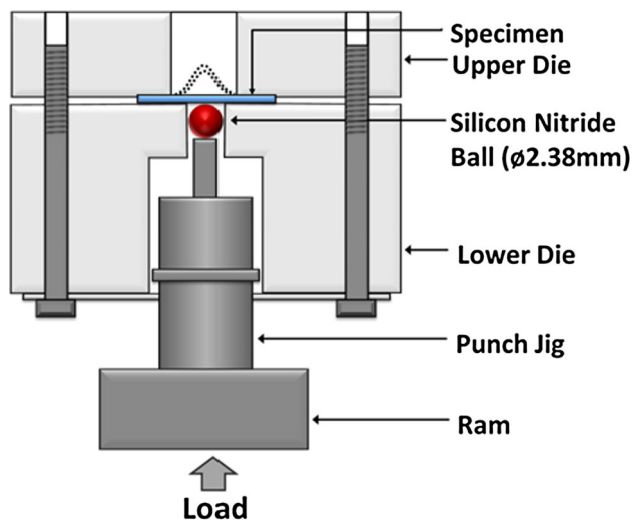


Fig. 1 Schematic illustration of small punch creep experimental setup

constant deflection SP test have been extended further for evaluating ductile to brittle transition temperature [5, 6], fracture toughness [7] and tensile properties such as fracture strain, yield stress and ultimate stress [8]. The second version of SP test operated in constant load mode measures the time dependence of specimen deflection under constant force and is known as small punch creep (SPC) test. The shape of the time deflection curve in SPC is analogous to conventional uniaxial creep curve and thus offers the potential to evaluate the creep deformation behavior of materials. Since the earliest work on SPC for evaluating high temperature creep as reported by Parker and James [9], during the past decade many researchers particularly Ule et al. [10], Komazai et al. [11] and Dobes and Milicka [12] have worked on the standardization of this test technique and its implication for establishing a correlation with uniaxial creep. Recently, a CEN code of practice for SPC test has been evolved which mainly deals with the test technique and testing procedure based on European research coordinated by the European Pressure Equipment Research Council (EPERC) under the Round-Robin testing program [13–15]. However, a crucial problem in the application of SPC test for the assessment of creep life is the knowledge of relationships between the results of this test and the conventional tests. At present, several studies have been carried out to establish these relationships based on empirical evaluations [16–18] and FEM analysis [19–21], but these are material specific and need further investigations.

During the past decade, tungsten alloyed high Cr ferritic grade P92 steel has been widely recognized as a potential material for elevated temperature applications in Ultra Super Critical (USC) power plants owing to its low

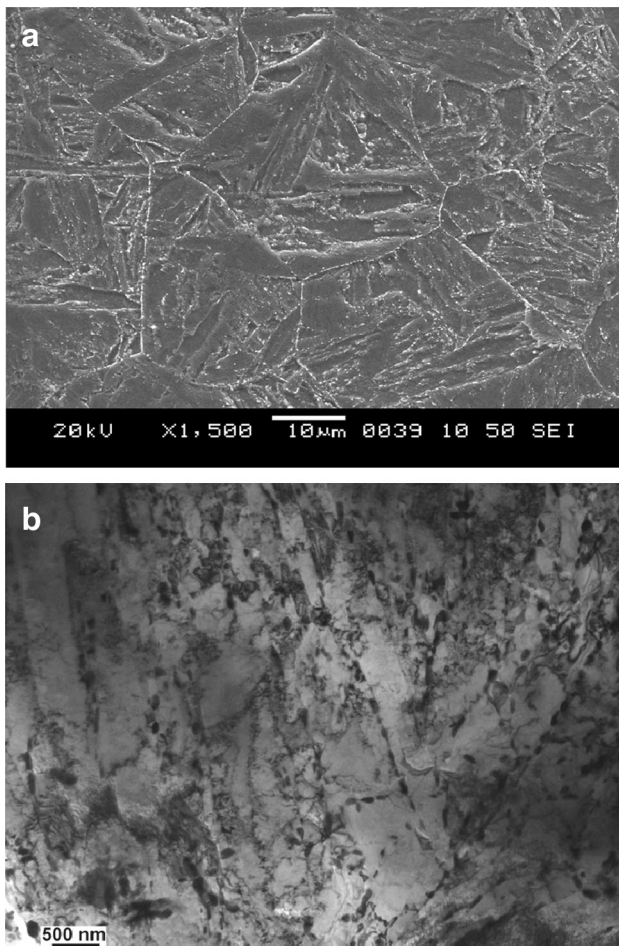
coefficient of thermal expansion, high thermal conductivity and resistance to thermal fatigue. P92 belongs to the third generation of modified 9Cr steel used in power generation industry and is a simple modification of P91 in which half of the Mo content is replaced by 1.8 wt% W along with other alloying elements such as Nb and V. This steel owes its high temperature creep strength to the tempered martensite lath structure, along with additional solid solution strengthening of the martensitic matrix by W addition and the precipitates of $M_{23}C_6$ type carbides ($M=Fe, Cr, Mo$) and MX type carbonitrides ($M=Nb, V$ and $X=C, N$) which are formed during the normalizing and tempering heat treatments as has been reported by Ennis and Filemonowicz [22]. As a result this steel has higher creep strength as compared to P91. Ennis et al. has also analyzed the relationship between creep rupture properties and microstructure of P92 steel and found that the creep strength is sensitive to microstructural variation [23] which in turn has been reported to be dependent on heat treatment process [24, 25]. The literature on the creep deformation behavior of P92 steel is mainly limited to uniaxial creep testing. The objective of the present paper is to investigate the suitability of SPC testing technique to characterize the creep deformation behavior of P92 steel. The results of SPC test have been analyzed using various constitutive creep equations. In addition, the study is also aimed at establishing correlation between the uniaxial creep parameters and SPC parameters by comparing uniaxial creep results with SPC results.

2 Materials

P92 steel involved in this investigation was procured in the form of rolled plate. The chemical composition of this steel analyzed by spectro-chemical analysis is given in Table 1. A bar of $60 \times 12 \times 12$ mm was machined from this plate in the rolling direction. The creep strength of the material is sensitive to normalizing and tempering heat treatment. The material was initially normalized (1050 °C for 30 min) and tempered (780 °C for 120 min) to homogenize the microstructure and then subjected to heat treatment consisting of normalizing at 1080 °C for 30 min followed by tempering at 740 °C for 60 min. The microstructure of this steel after normalizing and tempering consisted of tempered martensitic laths along with precipitates on the lath boundaries and prior austenitic grain boundaries as shown in Fig. 2. Fine precipitates were present in the interlath boundaries. SPC specimens were fabricated from the heat treated bar by electric discharge machining. The slices were grinded and subsequently polished by 1200 grit abrasive paper on both sides for a final dimension of $10 \times 10 \times 0.5$ mm with an accuracy of ± 0.003 mm.

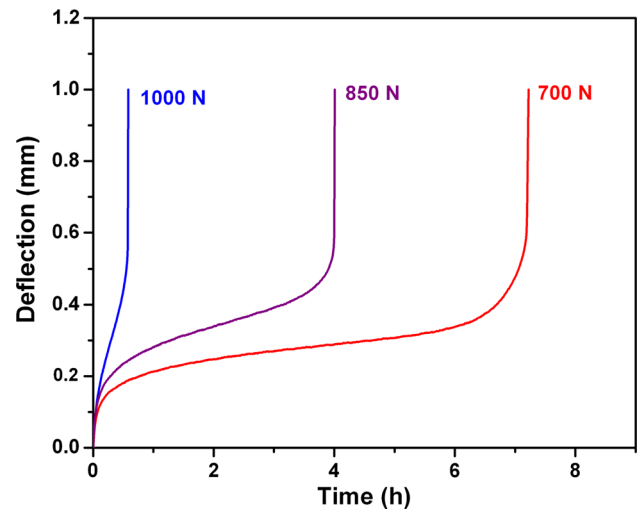
Table 1 Chemical composition (wt%) of P92 steel

Cr	C	Mo	W	Mn	Nb	V	N	Si	Cu	P	Al	S	B	Fe
9.38	0.11	0.50	1.94	0.38	0.07	0.21	0.041	0.023	0.016	0.012	0.007	0.003	0.002	Bal.

**Fig. 2** Microstructure of normalized (1080 °C × 30 min) and tempered (740 °C × 60 min) P92 steel. **a** SEM micrograph and **b** TEM micrograph

3 Small Punch Testing

The instrument used to perform the SPC experiments was a high temperature SPC machine of 2 kN load capacity. The system consists of a loading device, displacement measuring device, furnace, vacuum system, sample holder, silicon nitride (Si_3N_4) spherical ball of 2.38 mm diameter and a data logger. In order to prevent high temperature oxidation of the specimen, prior to the experiments the specimen chamber was evacuated and purged with argon gas and its flow was continued throughout the experiment. The SPC tests were conducted in constant load mode. The specimen was held in a specimen holder and load was applied by means of silicon nitride ball through ram

**Fig. 3** SPC curves at 600 °C for P92 steel at different loads

connected to loading device composed of a linear actuator coupled with a servo motor. The schematic diagram of SPC setup is shown in Fig. 1. The displacement was measured by means of a pulse encoder type displacement measuring device in the range of 0–5 mm. The SPC tests were conducted on P92 steel at temperature of 600 °C with accuracy of ± 1 °C under different load levels in the range of 1000–400 N.

4 Results and Discussion

4.1 SPC Results

The SPC curves of P92 steel at various load levels exhibiting the variation of specimen deflection with time are shown in Fig. 3. In general, the curves exhibit the typical three stages of creep similar to that of an ideal creep curve obtained from conventional uniaxial creep test. In SPC, after the instantaneous deflection, bending is the dominant deformation mode in primary stage which is characterized by a decrease in deflection rate, whereas membrane stretching is the prominent deformation mode during secondary and tertiary stages. During tertiary stage deflection rate accelerates on account of localization of deformation and nucleation and propagation of cracks until the final fracture. However, from Fig. 3 it is observed that a variation in load causes a change in the shape of the SPC curves. An increase in load accelerates the creep rate

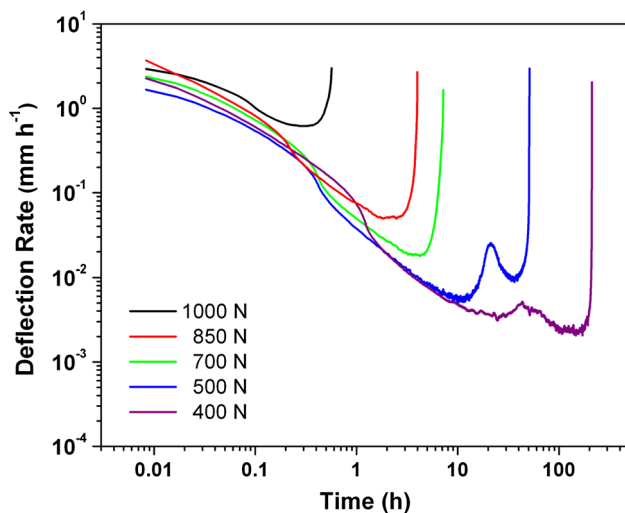


Fig. 4 Variation of SPC deflection rate versus time curves at different loads for P92 steel at 600 °C

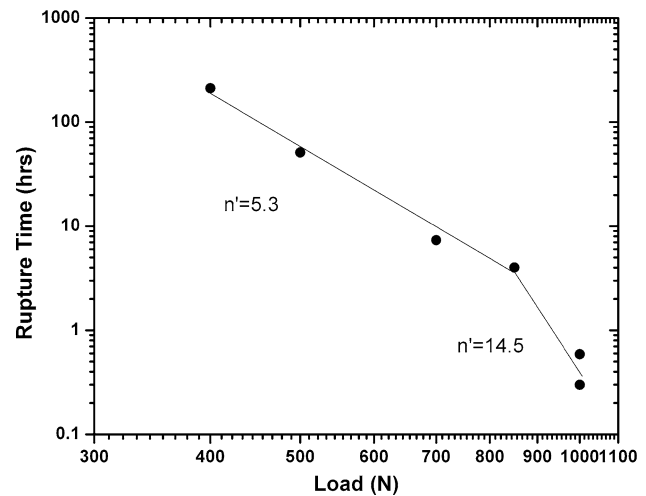


Fig. 6 Variation of rupture life with load for P92 steel at 600 °C

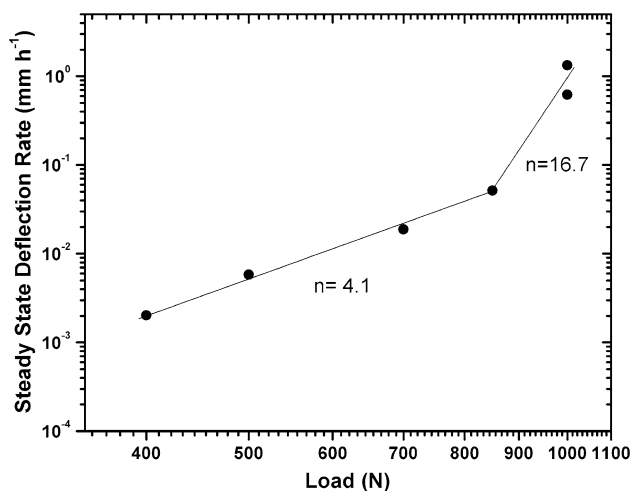


Fig. 5 Variation of minimum deflection rate with load for P92 steel at 600 °C (Norton's power law)

thereby decreasing the steady state range, such that at very high loads it is practically absent. Whereas, with decrease in load the creep rate decreases and the primary and steady state stage become clearly evident. A comparison of the deflection rates versus time curves shown in Fig. 4 clearly demonstrates that a decrease in load decreases the deflection rate by several magnitudes.

Minimum deflection rate is an important parameter that can be evaluated from SPC curves. A plot of minimum deflection rate as a function of load is shown in Fig. 5. The dependence of the minimum deflection rate on the applied load can be described by a power law relationship which is similar to Norton's power law used to express the creep deformation characteristics in conventional creep. The relationship is given by $\dot{\delta}_m = AF^n$ where $\dot{\delta}_m$ is the

minimum deflection rate, A is a temperature dependent constant, F is the load acting on specimen and n is load exponent. From Fig. 5 it is evident that P92 steel exhibits two slope behavior with each region obeying Norton's power law separately. The characteristic values of the exponent n in the low and high load regimes are found to be 4.1 and 16.7 respectively. The prevalence of distinct load regimes along with a large variation in the load exponent values clearly indicates a breakdown of creep strength. Similar two slope behavior is also seen in the log–log plot of variation of creep rupture life with load presented in Fig. 6. The load dependence of rupture life (t_r) also obeys a power law relation similar to that of Norton's power law as given by $t_r = A'F^{n'}$ where A' is a constant and n' is power law exponent. Two distinct values of load exponent $n' = 14.5$ in high load region and $n' = 5.3$ in the low load region confirms the breakdown of creep strength in this steel. The values of the load exponents for P92 steel in the two distinct load regimes for the load dependence of minimum deflection rate and rupture time are in agreement with the values of stress exponents reported in the literature for conventional uniaxial creep tests by Ennis et al. [23], Lee et al. [26] and Isaac et al. [27]. Similarity between the values of load exponents n and n' indicates that the mechanism for creep deformation and fracture are same as has been reported by Sklenicka et al. [28] and Choudhary et al. [29]. However, difference in the values of load exponents in the low and high load regions indicate a breakdown of creep strength in this steel. Lee et al. has associated the breakdown in creep strength with a transition from ductile transgranular fracture to brittle intergranular fracture with increasing creep life.

In order to investigate the creep deformation process of P92 steel the SPC ruptured specimens were investigated by

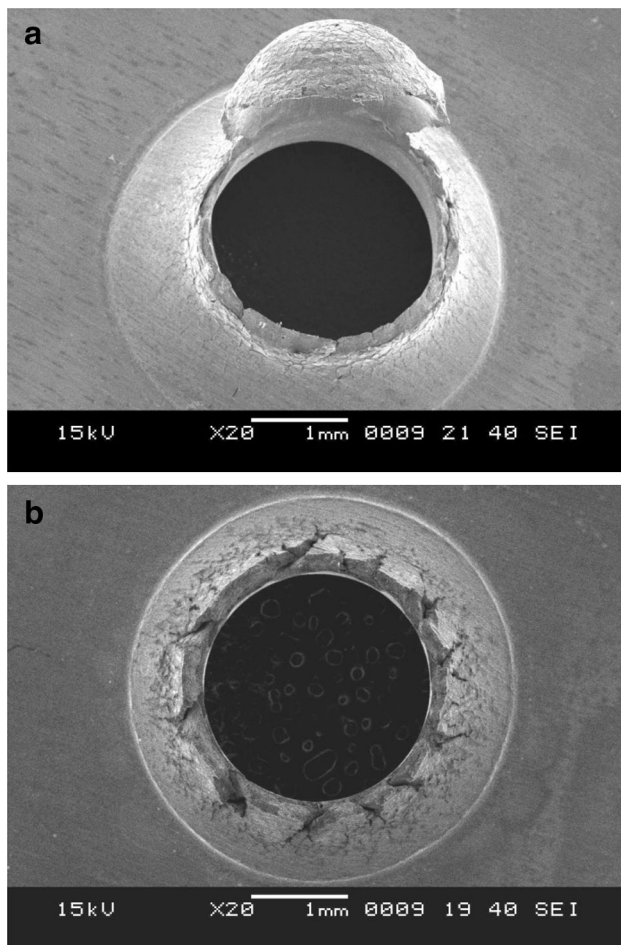


Fig. 7 Overview of SPC ruptured samples for P92 steel at 600 °C and different loads. **a** 1000 N and **b** 400 N

scanning electron microscopy (SEM). Figure 7 compares the SEM overview of SPC specimens fractured at different loads. Figure 7a clearly shows that SPC specimen deformed in the form of a hemispherical cup around the contact area of ball and final fracture occurred as result of a circumferential crack. During the SPC test when the ball initially comes in contact with the specimen surface, deformation of the specimen begins by elastic bending. This is followed by plastic bending during which a yield zone develops in the highly stressed parts of the specimen and spreads out radially through the specimen thickness. The deformation mode then exhibits a transition from plastic bending to membrane stretching and the yield front expands beyond the contact area of specimen and ball. The final fracture occurs near the edge of the hemisphere on account of localized necking which leads to the development and growth of a circumferential crack. In the SPC sample ruptured at high load (Fig. 7a) the cup is attached to the specimen by the last ligaments of the stretched cup accounting for a ductile fracture. As opposed to this in the

creep ruptured sample for long exposure time (Fig. 7b) the stretched cup has separated from the specimen. In addition to this, radial cracks are also seen around the circumferential crack indicating a brittle fracture and a change in rupture ductility with decrease in load.

The high magnification fractographs of these samples have also been investigated for deformation mechanism. The micrograph of the SPC specimen ruptured at high load of 1000 N (Fig. 8a) reveals uniform fracture surface with equiaxed dimple structure as shown in the inset image, indicating transgranular ductile fracture. Dimples are characteristic features of transgranular ductile fracture which are formed during creep as a result of nucleation, growth and coalescence of microvoids. With a decrease in load the fracture mode in SPC specimens exhibits a change from homogeneous fracture to an inhomogeneous and mixed mode consisting of ductile and cleavage parts as seen from Fig. 8b for 850 N. Also, the fracture surface for this sample can be divided into two distinct zones—labeled as region 1 and 2 in Fig. 8b. Region 1 is the outer ductile region wherein the fractured surface shows elongated dimples with one end continuous and other end stretched and open. The inner region 2 depicts a coarse and brittle nature. This indicates that the fracture may have originated in region 1 on account of shear stresses and terminated in region 2. In contrast to this, at still lower load of 400 N the fracture surface of SPC sample (Fig. 8c) is characterized by a uniform coarse appearance indicating a brittle intergranular fracture. The brittle fracture has been attributed to the formation of wedge cracks and r-type creep cavities along the grain boundaries in P92 steel [26]. From these micrographs it can be clearly recognized that the fracture mode exhibits a transition from ductile transgranular to brittle intergranular mode which can be associated with the breakdown of creep strength with an increase in creep exposure time.

Several explanations have been proposed in the literature in support of the change in the deformation mode and breakdown of creep rupture strength in P92 steel based on the contributions of various microstructural features. The important factors that determine the high creep strength of P92 steel are (i) solid solution strengthening by W (ii) high dislocation density induced by martensitic transformation and (iii) $M_{23}C_6$ type carbides (M-Fe, Cr, Mo) and MX type carbonitrides. $M_{23}C_6$ carbides are precipitated preferentially on the prior austenitic grain boundaries and lath boundaries, whereas fine MX(C, N) precipitates of Nb carbonitrides and V nitrides are within the martensitic laths. These precipitates act as obstacles for the dislocation movement during creep thereby retarding the subgrain growth and consequently increasing the creep strength. An increase in creep rupture life causes a reduction in dislocation density and accelerates the coarsening of

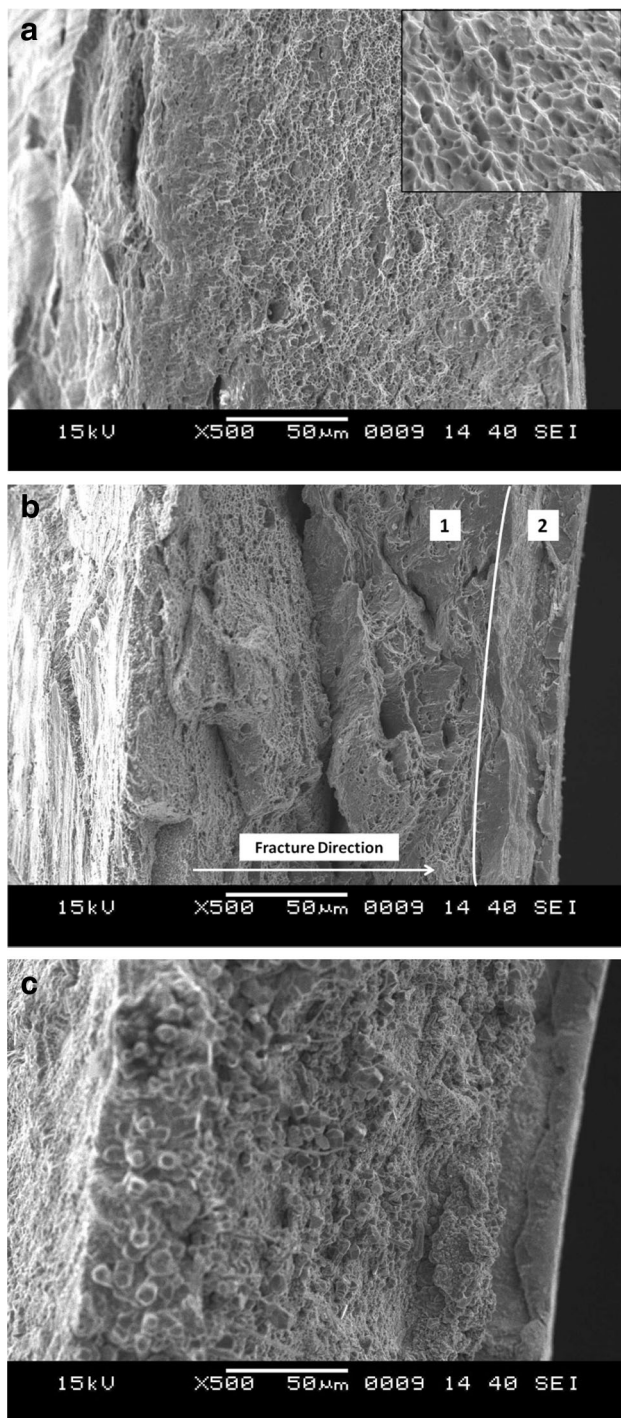


Fig. 8 SEM images of fracture surface of SPC samples at 600 °C and different loads. **a** 1000 N, **b** 850 N, and **c** 400 N

$M_{23}C_6$ carbides along with the precipitation of Laves phase (M_2X) at the expense of W from the matrix. The removal of W from the matrix leads to loss of creep rupture strength as has been explained by Muraki et al. [30]. Apart from this it has also been shown that coarse $M_{23}C_6$ carbides and Laves phase are preferential nucleation sites for creep cavitation [23, 24]. A study by Lee et al. [26] on the causes

of breakdown of creep strength in P92 steel reveals that coarsening of Laves phase by Ostwalds ripening above a critical size triggers a transition in fracture mode on account of nucleation of cavities, their growth and coalescence to form grain boundary microcracks which bring about brittle intergranular fracture.

Ashby et al. [31] have demonstrated in fracture mechanism maps that the transition in fracture mode is associated with a change in activation energy. This has also been confirmed in several investigations of 9 % Cr ferritic steels wherein decrease in the value of stress exponent (n) and apparent activation energy have been reported with an increase in rupture life [26, 32]. Choudhary et al. [32] rationalized the different values of stress exponents and apparent activation energy in the low and high stress regimes of P92 steel into a single value by invoking the concept of resisting stress and suggested that creep behavior is controlled by dislocation climb in both the stress regimes. Based on the above discussion it can be concluded that the two slope creep behavior of P92 steel observed from SPC test exhibits good correlation with conventional uniaxial creep test. The high value of load exponents in the high load regime indicate the strengthening effects of various microstructural features whereas the decrease in exponent value for long terms tests points towards the deterioration of creep strength on account of decrease in dislocation density, coarsening of $M_{23}C_6$ carbides and precipitation of Laves phase. This further suggests that creep behavior is load controlled in high load regime, while for low load regime creep deformation is governed by diffusion controlled phenomenon which leads to microstructural degradation.

4.2 Correlation Between SPC Parameters and Uniaxial Creep Parameters

In order to utilize the potential of SPC tests for characterizing the creep behavior of materials, it is imperative to establish quantitative correlations between conventional creep data and SPC data. In SPC test the important parameters are load and minimum deflection rate whereas in convention uniaxial creep test these are stress and minimum creep rate. From the above discussion on creep results of P92 steel it is apparent that the relationships between load and various SPC parameters like minimum deflection rate ($\dot{\delta}$) and rupture time (t_r) are similar to that of conventional uniaxial creep tests. A comparative plot of creep rupture life with respect to load and stress determined from SPC and conventional creep tests respectively is shown in Fig. 9. Both the test data exhibits a linear relationship, but no direct correlation is evident between load and stress. Therefore, the challenge is to find the equivalence between load and stress for the applicability of SPC

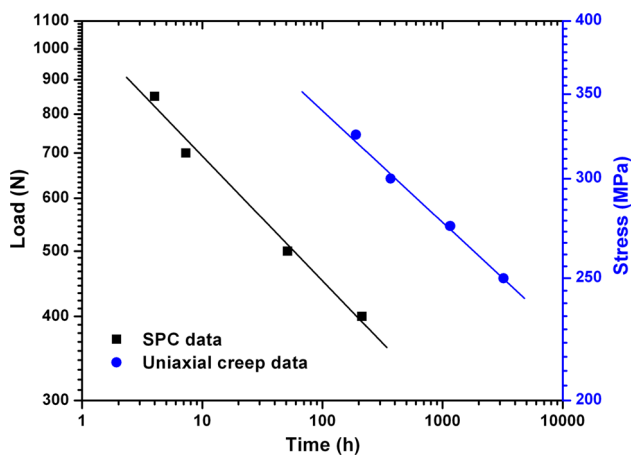


Fig. 9 Dependence of rupture time on load and stress for SPC and uniaxial creep tests for P92 steel at 600 °C

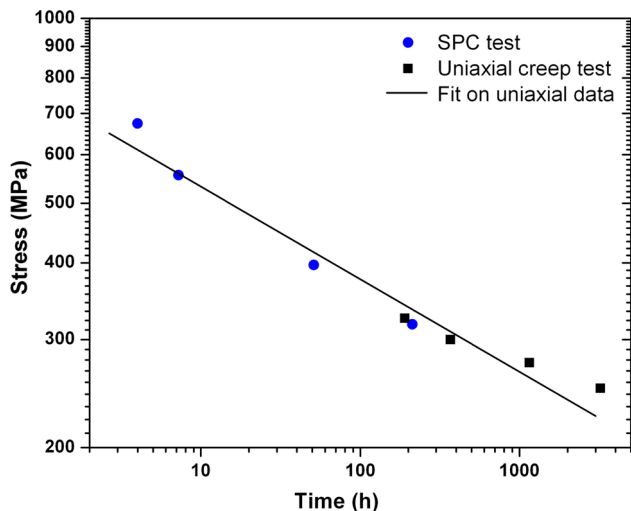


Fig. 10 Correlation between SPC and uniaxial rupture life for P92 steel at 600 °C

test as an alternative to uniaxial creep tests. Furthermore since the state of stress in SPC is multiaxial and differs from that of uniaxial creep tests, the relationships proposed in the literature to correlate load and stress for the same rupture life are based on different approaches like finite element modeling calculations, equations derived from stretching membrane theory proposed by Chakraborty [33] and empirical evaluations. One such relation [34] derived from the stretching membrane theory and applicable to most materials is given by:

$$F/\sigma = K \cdot R \cdot t^2/h \cdot D \tag{1}$$

where F is SPC load, σ is uniaxial stress, K is a geometrical constant, R is the diameter of ball punch, t is the specimen thickness, h is the radius of receiving hole and D is the ductility factor for the material in test temperature and load

range. In the above equation since the values of material constant D and geometrical parameter K are not known, it can be simplified further as follows $F/\sigma = \alpha$ and the value of α can be determined empirically by comparing SPC and uniaxial creep rupture life as recommended by CEN [35]. Based on this method the rupture life data from SPC and uniaxial creep tests was compared for the lower stress exponent values ($n, n' = 4.1, 5.3$). The corresponding graph for the same rupture life data for SPC and uniaxial test is shown in Fig. 10 and the value of α is found to be 1.25. The plot shows an excellent correlation between SPC load and uniaxial stress for the same rupture life.

The correlation between SPC load and uniaxial creep stress has also been evaluated based on following equations as proposed in the European code of practice.

$$F/\sigma = [2\pi t(R + t/2)]\alpha \tag{2}$$

$$\alpha = A + B \epsilon_c$$

where R is the indenter radius, t is the specimen thickness, ϵ_c is the average creep strain and the value of $A = 0.24$ and $B = 0.53$, as proposed in the code of practice. Taking the average value of creep strain for P92 steel determined from uniaxial creep tests as $\epsilon_c = 6\%$ the F/σ ratio for P92 steel was found to be 1.23. This value is found to be in accordance with that determined from the comparison of SPC and conventional creep data.

Similarly, the correlation between minimum deflection rate and minimum creep rate can be established based on Monkman–Grant relationship. In conventional creep, Monkman–Grant describes the relation between minimum creep rate and time to rupture as follows:

$$\log t_f + m_C \log \dot{\epsilon} = C_C \tag{3}$$

where t_f is rupture time, $\dot{\epsilon}$ is minimum creep rate and m_C and C_C are constants. Detailed studies by Dobes and Milicka [36] on the applicability of this relation to SPC tests have shown that the dependence of minimum deflection on time to fracture can also be described by relation analogous to Eq. 3.

$$\log t_f + m_S \log \dot{\delta} = C_S \tag{4}$$

where $\dot{\delta}$ is minimum deflection rate and m_S and C_S are constants. Figure 11 shows the dependence of time to rupture on minimum deflection rate and minimum creep rate. The values of the above mentioned constants evaluated from these plots are given in Table 2. The data for both SPC and uniaxial creep tests lie on straight lines and the values of m_S and m_C are close to 1 indicating the validity of these relations for estimating the rupture time for long duration tests. Based on Eqs. (3) and (4), the minimum deflection rate and creep rate can be correlated as proposed by Milicka and Dobes [36].

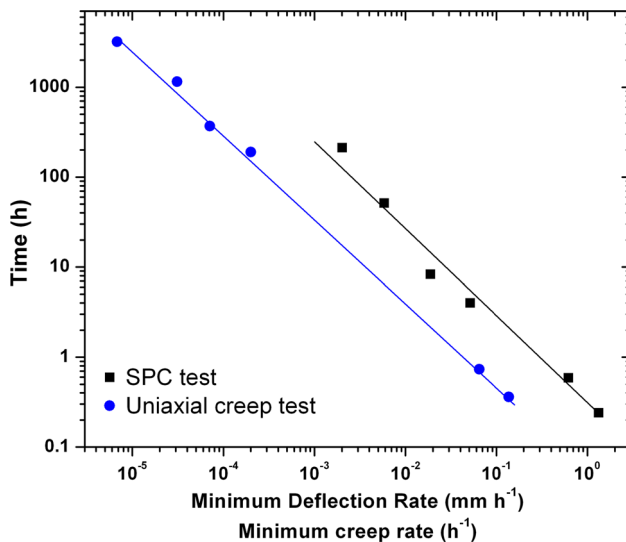


Fig. 11 Monkman–Grant relation exhibiting dependence of rupture time on minimum deflection rate and minimum creep rate for P92 steel at 600 °C

Table 2 Monkman–Grant constants of P92 steel determined by SPC and uniaxial creep tests

Test	m_c, m_s	C_c, C_s	r^2
Uniaxial creep	0.93	0.05	0.997
SPC	0.96	0.31	0.988

$$\dot{\epsilon} = 10^{(C_c - C_s)/m_c} (\dot{\delta})^{m_s/m_c} \quad (5)$$

As the values of m_s and m_c are same the correlation between minimum deflection rate and minimum creep rate for P92 steel can then be given by a more general equation as follows:

$$\dot{\epsilon} = 0.525\dot{\delta} \quad (6)$$

The excellent correlations observed between SPC and conventional creep data indicate the applicability of SPC technique for evaluating the creep behavior of materials. However, since these correlations are totally empirical in nature, it is essential to further validate them by finite element analysis.

5 Conclusions

In this investigation the creep deformation behavior of P92 steel at 600 °C was evaluated by employing SPC technique. The SPC data was compared with uniaxial creep data in order to determine the correlations between the two. Following conclusions can be drawn based on the present study:

- (i) The shapes of the SPC curves in P92 steel demonstrated delineated primary, secondary and tertiary stages of creep.
- (ii) The load dependence of minimum deflection rate obeyed Norton's power law exhibiting well defined two slope behavior with distinct values of load exponent in high and low load regimes. Similar two slope behavior was also evident in the load dependence of time to rupture which also obeyed a power law indicating a change in creep deformation.
- (iii) Fractography study confirmed a transition in creep deformation mode on account of microstructural changes from a transgranular ductile fracture at high loads to intergranular brittle fracture at low loads, correlating well with the two slope behavior.
- (iv) The correlation between SPC load and uniaxial creep stress for the same rupture time followed a simple linear proportionality equation with a value of $\alpha = 1.25$.
- (v) Monkman–Grant type equation which relates minimum deflection rate and time to rupture was found to be valid for SPC data.

Acknowledgments The authors would like to acknowledge UGC-DAE-CSR for the financial support of this project. The authors also wish to express their gratitude to UGC-DAE-CSR center, Kalpakkam Node for providing the experimental facilities and Mr. N. S. Thampi for technical support.

References

1. Lucas G E, *J Nucl Mater* **117** (1983) 327.
2. Lucas G E, Okada A, and Kiritani M, *J Nucl Mater* **141** (1986) 532.
3. Manahan M P, Argon A S, and Harling O K, *J Nucl Mater* **103** (1981) 1545.
4. Huang F H, Hamilton M L, and Wire G L, *Nucl Technol* **57** (1982) 234.
5. Baik J M, Kameda J, and Buck O, *Scr Metall Mater* **17** (1983) 1443.
6. Kohse G, Ames M, and Harling O K, *J Nucl Mater* **141–143** (1986) 513.
7. Mao X, Shoji T, and Takahashi H, *J Test Eval* **15** (1987) 30.
8. Mao X, and Takahashi H, *J Nucl Mater* **150** (1987) 42.
9. Parker J D, and James J D, *ASME PVP* **279** (1994) 167.
10. Ule B, Sustar T, Dobes F, Milicka K, Bicego V, Tettamanti S, Maile K, Schwarzkopf C, Whelan M P, Kozlowski R H, and Klaput J, *Nucl Eng Des* **192** (1999) 1.
11. Komazai S, Hashida T, Shoji T, and Suzuki K, *J Test Eval* **28** (2000), 249.
12. Dobes F, and Milicka K, *J Test Eval* **29** (2001) 31.
13. European Creep Collaborative Committee, ECCC Recommendations—Volume 3, Chapter 3, S. Brett (2005).
14. Small Punch Test Method of Metallic Materials, CEN Workshop Agreement, CWA. 15627: 2006 E, CEN, Brussels, Belgium (2006).
15. Blagoeva D T, and Hurst R C, *Mater Sci Eng A* **510–511** (2009) 219.

16. Dobes F, and Milicka K, *Int J Press Vessel Pip* **83** (2006) 625.
17. Dobes F, and Milicka K, *Mater Sci Eng A* **510–511** (2009) 440.
18. Dobes F, and Milicka K, *Mater Charact* **59** (2008) 961.
19. Zhai P C, Hashida T, Komazaki S I, and Zhang Q J, *J Test Eval* **33** (2005) 298.
20. Ling X, Zheng Y, You Y, and Chen Y, *Int J Press Vessel Pip* **84** (2007) 304.
21. Zhou Z, Zheng Y, Ling X, Hu R, and Zhou J, *Mater Sci Eng A* **527** (2010) 2784.
22. Ennis P J, and Filemonowicz A C, *Sadhana* **28** (2003) 709.
23. Ennis P J, Zielinska-Lipiec A, Wachter O, and Filemonowicz A C, *Acta Mater* **45** (1997) 4901.
24. Klueh R L, *Int Mater Rev* **50** (2005) 287.
25. Wang S S, Peng D L, Chang L, and Hui X D, *Mater Des* **50** (2013) 174.
26. Lee J S, Armaki H G, Maruyama K, Muraki T, and Asahi H, *Mater Sci Eng A* **428** (2006) 270.
27. Isaac E I, Choudhary B K, Palaparti D R, and Mathew M D, *Proc Eng* **55** (2013) 64.
28. Sklenicka S V, Kucharova K, Svoboda M, Kloc L, Bursk J, and Kroupa A, *Mater Charact* **51** (2003) 35.
29. Choudhary B K, and Samuel E I, *J Nucl Mater* **412** (2011) 82.
30. Muraki T, Hasegawa Y, and Ohgami M, *Key Eng Mater* **171–174** (2000) 499.
31. Ashby M F, Gandihi C, and Taplin D M R, *Acta Mater* **27** (1979) 699.
32. Choudhary B K, Phaniraj C, Bhanu Sankara Rao, and Manna S L, *ISIJ Int* **41** (2001) S73.
33. Chakrabarty J, *Int J Mech Sci* **12** (1970) 315.
34. Hurst R C, Stratford G C, and V. Bicego, in Proceedings of ECCC Creep Conference, London (2005) 349.
35. Small Punch Test Method for Metallic Materials Part 1: a code of practice for small punch testing at elevated temperatures, Report No. CEN/WS 21 (2005).
36. Dobes F, and Milicka K, *Mater Sci Eng A* **336** (2002) 245.